The effect of cyclic-loading generated intergranular strains on the creep deformation of a polycrystalline material

Journal Item

Materialia 7 (2019) 100385

Contents lists available at ScienceDirect

Materialia

journal homepage: www.elsevier.com/locate/mtla

Full Length Article

The effect of cyclic-loading generated intergranular strains on the creep deformation of a polycrystalline material

A.A. Mamun[a,b,*], R.J. Moat[a], J. Kelleher[c], P.J. Bouchard[a]

[a] Engineering and Innovation, The Open University, Walton Hall, Milton Keynes MK7 6AA, UK
[b] Department of Mechanical Engineering, University of Bristol, Bristol BS8 1TR, UK
[c] ISIS Facility, Rutherford Appleton Laboratory, Didcot, Oxford OX11 0QX, UK

ARTICLE INFO

Keywords:
Creep
Intergranular strain
Stainless steel
Neutron diffraction
Back-stress
Plasticity
Cyclic loading

ABSTRACT

Intergranular strains are generated due to the incompatible deformations at grain length-scales during elastic and inelastic loading in a polycrystalline material. Estimating the effects of intergranular strains on the creep life of the material is of interest for accurate life prediction of high-temperature structural systems. In this study, the effect of the cyclic loading generated intergranular strains on the creep deformation behaviour of Type 316H austenitic stainless steel was studied using in-situ neutron diffraction. The load-controlled creep dwells introduced at various positions during tension-compression cyclic loading with different intergranular strain state but under the same applied stress showed markedly different behaviours. It is inferred that the intergranular strains are a significant contributor to the observed differences in creep deformation behaviour. Comparing the evolution of intergranular strains in various grain families during plastic and creep deformation, it was found that the grain families which deformed relatively more or less during plastic deformation behaved similarly during creep deformation. The present work shows that intergranular strains, which contribute to accelerating/decelerating creep deformation rates, need to be accounted for in current creep life assessment procedures, to obtain a more realistic creep deformation prediction under cyclic loading conditions.

1. Introduction

The life of power generation plant operating at high-temperatures ($> 0.4\ T_m$) can be limited by creep deformation and damage of critical structural components. High-temperature assessments [1,2] of the integrity of these components under operational loading conditions provide crucial information for plant lifetime management, including inspection planning, avoiding costly repairs, premature shutdown or, at worst, disastrous failure. The monotonic creep deformation behaviour of commonly used high-temperature materials is well studied. However, service loading in power generation plant is complex in nature owing to plant start-up/shut-downs and electricity demand following cycles with extended steady-state constant load periods. This type of loading history subjects material to tension-compression stress–strain cycles with creep dwells that can occur at the peak stress position of the loading cycle or at an intermediate stress in the cycle. The creep-fatigue lifetime of materials exposed to such loading, where the number of fatigue cycles is low, is dominated by creep accumulated during dwell periods [3]. It is important therefore to be able to characterise creep deformation and damage developed during dwells starting anywhere in the stress–strain cycle.

High-temperature assessment procedures, for example, R5 Volume 2/3 [1], use the start of dwell stress as the main determinant to characterise the creep deformation during such a dwell. This start of dwell stress is calculated using an empirically constructed saturated cyclic stress–strain curve. It has been shown that such empirical prediction of creep deformation can be overly conservative for dwells introduced at the intermediate position of the cyclic loading [4]. This is because the creep deformation behaviour is not only dictated by the start of dwell stress but also by the material hardening and the internal stress state developed during the preceding plastic cyclic loading and how these evolve during the creep dwells [5].

Therefore, the simplistic empirical models used to explain creep and relaxation dwell behaviour after different pre-straining conditions often fail to fully capture the experimental response. A mechanistic modelling approach incorporating the underlying mechanisms of plasticity-creep interaction is therefore needed to quantify the creep response changes caused by prior deformation [6]. Several continuum and microstructure based creep models [7–9] have been developed which attempt to capture such understanding, however, traditional continuum approaches are limited in their ability to account for the influence of local variations at the inter and intra granular scales [10]. A common

* Corresponding author at: Department of Mechanical Engineering, University of Bristol, Bristol BS8 1TR, UK.
E-mail address: abdullah.mamun@bristol.ac.uk (A.A. Mamun).

https://doi.org/10.1016/j.mtla.2019.100385
Received 23 April 2019; Accepted 23 June 2019
Available online 28 June 2019

approach adopted in analytical [11–13] and finite element (FE) models [11,14] for estimating the creep deformation rate of materials under cyclic loading conditions is to use a concept termed 'back-stress' to adjust the applied stress. At a microstructural level, back-stress refers to the stress associated with local strains arising from long-range interactions of mobile dislocations whilst at a continuum mechanics level, the back-stress corresponds to the translation of the yield surface origin during kinematic hardening. The existence of back-stress is well evidenced from various deformation phenomena in metals such as the Bauschinger effect [15], anelasticity and creep rate changes during transient creep processes [16] etc. However, evaluation of how the back-stress evolves, particularly at the grain length scale, and how it affects subsequent creep deformation behaviour of polycrystalline material is not well understood.

In polycrystalline material like type 316H stainless steel, elastic and plastic deformation is anisotropic. Therefore, depending on their crystallographic orientation with respect to the loading axis, grains deform at different magnitudes of stress (elastic anisotropy) and yield at different applied stress (plastic anisotropy). These heterogeneities in deformation of the grains create an internal "pull and push" state described as "intergranular (IR) stress". These IR stresses significantly contribute to the back-stress and, depending on the magnitude and direction (tensile or compressive), can either increase or decrease the effective stress controlling the creep deformation rate in type 316H stainless steel [17,18]. Microplasticity can also influence the damage initiation and development in material [19]. Studies have been reported investigating the evolution of IR stress during high-temperature monotonic plastic loading [20], but there is a gap in understanding of how plasticity generated IR stresses affect subsequent creep behaviour. Chen et al. [21] studied the evolution of lattice strains in different grain families at different stages of creep deformation in type 316H stainless steel and reported the magnitude of IR strains to be a function of the total inelastic strain in the material. Rao et al. [22] reported compressive IR stresses to be a major contributor to anelastic creep strain recovery in type 316H stainless steel. Wang et al. [23] measured the evolution of lattice strains during creep dwells under different elastic-follow-up factors and found that under constant load control, the lattice strains in different grain families remained constant.

In this paper, we report findings from a novel study investigating the evolution of IR strains during cyclic plastic loading and those effects on subsequent load-controlled creep deformation behaviour in type 316H stainless steel at 650 °C. First, the generation of IR strains in different grain families (i.e. groups of grains having common crystallographic lattice planes oriented normal to a particular axis) is measured during monotonic and cyclic loading. The effect of the prior induced IR strain state on the creep deformation rate is then investigated by introducing creep dwells at 3 different positions in the cyclic loading curve but at the same start-of-the dwell stress. The corresponding changes in the dislocation structures at the start of the creep dwells are also investigated. To the best of our knowledge, this is the first study reported investigating the role of cyclic loading generated IR strains on the creep deformation behaviour in a polycrystalline material.

2. Materials and methods

The test specimens were machined from virgin AISI Type 316H austenitic stainless-steel bar and then solution heat-treated (1050 °C heat soak for 1 h followed by a water quench). The test specimens were cylindrical and had a gauge diameter, gauge length and total length of 8 mm, 14 mm and 74 mm, respectively. The chemical composition of the material determined by optical emission spectroscopy (OES) is presented in Table 1.

The evolution of lattice strains in several grain families was measured during the tests using an in-situ neutron diffraction technique. A grain family is defined as a set of grains having a similar crystallographic orientation, of which the corresponding hkl plane normal lies parallel to the scattering vector of diffraction. The experiment was conducted at the Engin-X Time of Flight (ToF) neutron diffraction instrument [25] at the Rutherford Appleton Laboratory, UK. Using the ToF technique, the change of lattice spacing between crystallographic planes can be measured for a number of grain families simultaneously from which the elastic lattice strains for various grain families can be calculated using equation below.

Table 1
Composition of the type 316H austenitic steel studied determined using optical emission spectroscopy (OES).

Element	C	Si	Mn	P	S	Cr	Cu	Ni
% wt	0.07	0.41	0.98	0.024	0.016	17.2	0.14	11.5
Element	Mo	Co	W	V	Al	As	Fe	
% wt	2.3	0.07	0.05	0.04	0.003	0.01	Bal.	

$$\varepsilon_{hkl} = \frac{d_{hkl} - d_{0\ hkl}}{d_{0\ hkl}} \quad (1)$$

Here, ε_{hkl} is the lattice strain for a {hkl} grain family, d_{hkl} is the lattice spacing and $d_{0\ hkl}$ is the stress-free lattice spacing of the corresponding grain family.

The cyclic creep tests were conducted at 650 °C using an Instron 100 kN stress rig with a radiant furnace [25]. The test specimen temperature was monitored continuously with a K-type thermocouple spot welded to the centre of the gauge length (only one thermocouple could be used owing to the short gauge length). The macroscopic strain was measured using an Instron high-temperature extensometer attached directly to the gauge length of the specimen using a spring and tension strings combination. A sample gauge volume of $4 \times 4 \times 7.17\ mm^3$ was used for the neutron measurements. A "back-to-back" counting time of 300 and 600 s was used to collect neutron data during cyclic and creep dwell phases respectively. During cyclic loading, neutron diffraction data were collected by holding the strain constant at a point to avoid the introduction of any creep strain and therefore allowing the stress to relax slightly whereas, during creep dwells, data were collected by holding the stress constant.

Three different specimens, with identical properties, were tested during the *in-situ* experiment. For each test, the specimen was first mounted in the stress rig and heated to 650 °C using the radiant furnace. The specimen was then subjected to a small stabilising load (5 MPa stress) and the reference lattice spacings (d_0) measured for the grain families. The different specimen was then subjected to different loading sequence as shown in Fig. 1. A strain rate of $7 \times 10^{-6}\ s^{-1}$ was used for all 3 tests. In each test (using different specimens), the loading was stopped at different points in the loading cycle, shown as point A, B and C in Fig. 1. A load-controlled creep dwell of ~15 h was introduced instantly at these points. The three tests are termed as test A, test B and test C corresponding with the interruption points.

Test A: the specimen was loaded in tension to 1% strain at 650 °C and a load-controlled creep dwell introduced with a start of dwell stress of 120 MPa.

Test B: the specimen was cyclically loaded over $a \pm 1\%$ strain range at 650 °C. Upon reaching 1% peak strain in the 2nd cycle, the load reduced to 120 MPa and a load-controlled creep dwell introduced.

Test C: the specimen was cyclically loaded over $a \pm 1\%$ strain range at 650 °C. The loading was stopped at 120 MPa while reloading from −1% strain on the 3rd cycle, and a load-controlled creep dwell introduced.

A set of identical tests were also conducted *ex-situ* using an Instron high-temperature stress rig at the Open University high-temperature laboratory. The tests were interrupted at cyclic loading history of A, B and C as shown in Fig. 1. After the load interruption, the specimens were cooled quickly under load in order to preserve the dislocation structures. The specimens were then sectioned radially, and smaller sized specimens extracted for dislocation analysis. A JEOL JEM 2100 microscope

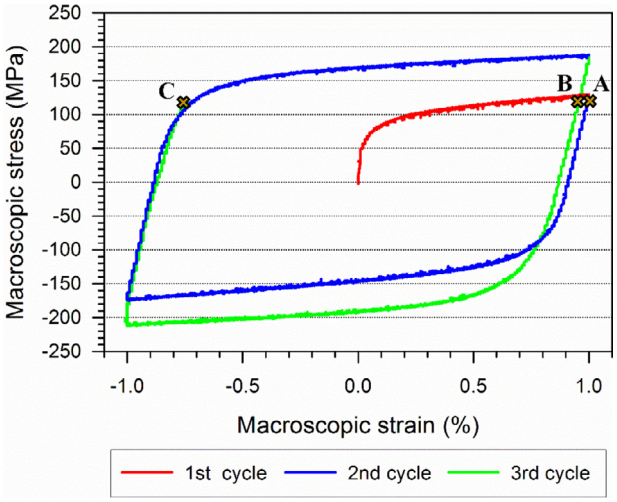

Fig. 1. Cross marked A, B and C are the points at which the loading was interrupted, and a load-controlled creep dwell introduced for the three tests conducted. Identical but separate specimens were used for the tests. The data for tests A, B and C are marked in a different colour for better visualisation.

was used for Transmission Electron Microscope (TEM) investigations. Foil specimens of ~100 μm thickness were prepared by electropolishing in a solution of 5% perchloric acid in methanol at −60 °C using a 20 V electric current. A double tilt specimen holder was used for the TEM imaging, such that images from multiple crystallographic planes are obtained.

3. Results

3.1. Evolution of IR strains during monotonic and cyclic loading

During uniaxial tensile/compressive deformation of undeformed type 316H stainless steel, the {220} grain family usually yields first, the {200} grain family last and the {311} grain family generally exhibits grain average behaviour [20]. Results from these three grain families alone are presented and discussed in the remainder of this paper as they represent the behaviours of plastically weaker, stronger and average grains in type 316H austenitic stainless steel. Fig. 2(a) plots the IR strains (IR) vs macroscopic stress measured by neutron diffraction during a uniaxial monotonic tensile test of Type 316H stainless steel at a temperature of 650 °C.

A number of interesting features regarding the elastic and plastic anisotropic deformation of 3 different grain families can be observed from this simple test. First, elastic lattice strain in the 3 grain families increases linearly with applied macroscopic stress up to ~60 MPa. Differences between the slopes of these lines are due to the differences in crystallographic stiffness of the grain families (elastic anisotropy). Thereafter, the {200} grain family behaviour is observed to deviate from linearity in a tensile sense, the {220} grain family in a compressive sense and the {311} grain family stays linear. The linear response, that is the ideal elastic lattice strains for each grain family, was constructed using experimentally measured diffraction elastic constants from [20]. At ~100 MPa, the elastic strain in the {220} grain family can be observed to stop increasing with increasing applied stress, implying that the grains belonging to this family are now deforming plastically, while the other 2 families are still deforming elastically (plastic anisotropy). The plastic deformation in the {220} grain family is constrained by neighbouring elastically deforming grains and this creates IR stresses. If the applied load is taken off, the lattice strains in the grain families will unload elastically resulting in tensile and compressive residual strains in the {200} and {220} grain families respectively, as can be seen from the imaginary solid unloading lines in Fig. 2(a). The magnitude of the IR strains

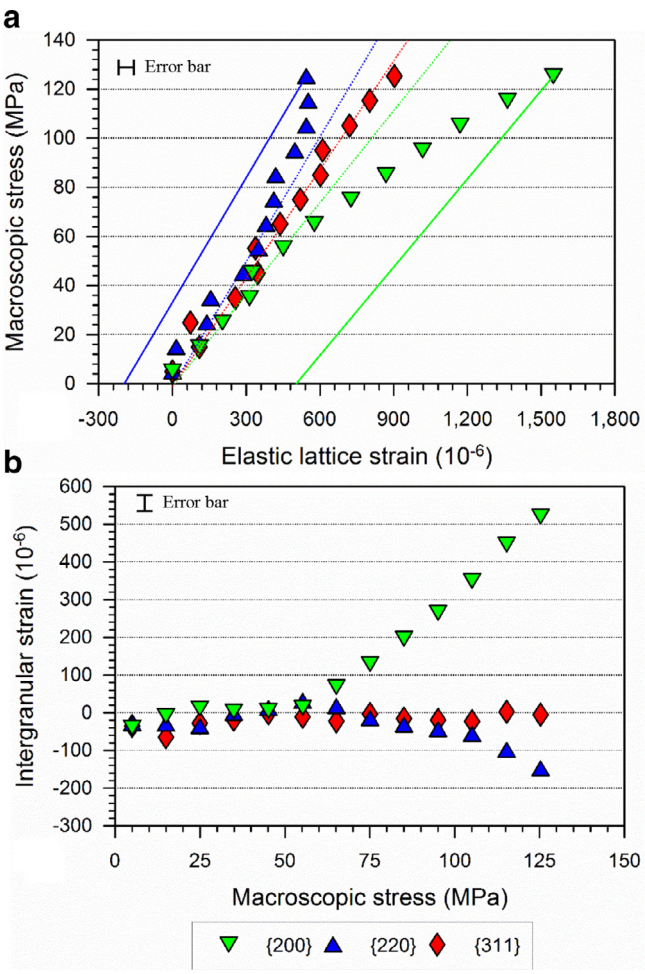

Fig. 2. (a) The axial elastic lattice strain in different grain families during tensile loading of type 316H austenitic stainless steel at 650 °C. The lattice strains in the {200} and the {220} grain families are observed to deviate from ideal linear elastic behaviour (shown by dotted lines) due to elastic and plastic anisotropy. Elastic unloading lines are shown for the {200} and {220} grain families that indicate the level of trapped residual strains at zero macroscopic stress. (b) Evolution of IR strains calculated from the difference of the elastic lattice strain and the ideal elastic lattice strain (calculated using diffraction elastic constants for the respective grain families) for the same tensile test.

created due to the elastic-plastic anisotropy can be estimated from the deviation of the elastic stress–strain line from the ideal elastic line. As this deviation of the elastic lattice strains from that ideal elastic line is due to the elastic and plastic anisotropy, these can be used as a measure of the IR strains in the material. The axial IR strains from the tensile test are plotted in Fig. 2(b). The IR strains can be observed to be negligible up to ~60 MPa of applied stress, following which tensile and compressive IR strains are generated in the {200} and the {220} grain families respectively. The magnitude and nature of the IR strains match quite well with those reported for up to 200 MPa applied stress by Daymond et al. [20].

Fig. 3 shows the measured evolution of IR strains in the 3 grain families during tension-compression cyclic loading over $a \pm 1\%$ strain range of type 316H stainless steel at 650 °C. During the first tension one-quarter cycle, tensile and compressive IR strains are generated in the {200} and the {220} grain families respectively and then reverse in the direction in a synchronised sense with the macroscopic deformation. The IR strains in the {311} grain families are compressive and remain small in magnitude irrespective of the macroscopic tension-compression loading. The IR strains in all 3 grain families increase in magnitude with

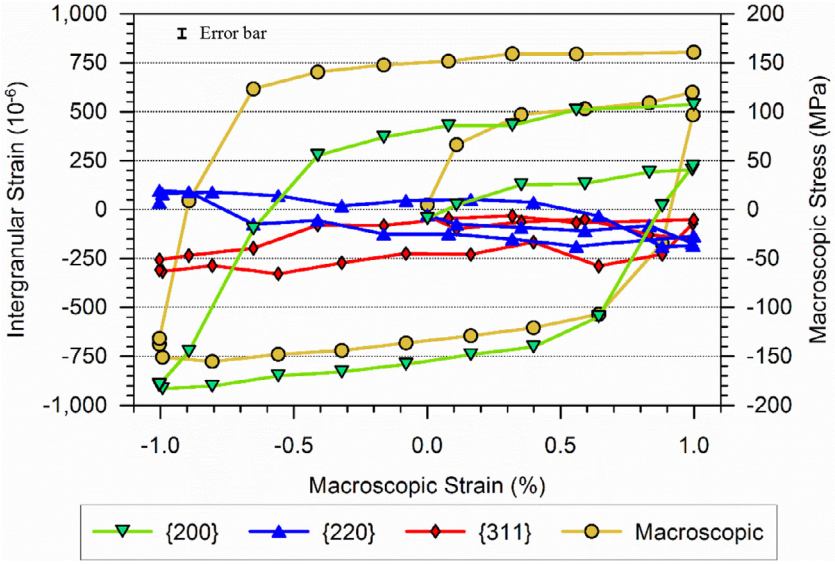

Fig. 3. Variation of axial IR strains in 3 grain families during tension-compression cyclic loading of type 316H stainless steel at 650 °C. The macroscopic loading curve to be read with right *Y*-axis and the IR strain curves to be read with left *Y*-axis.

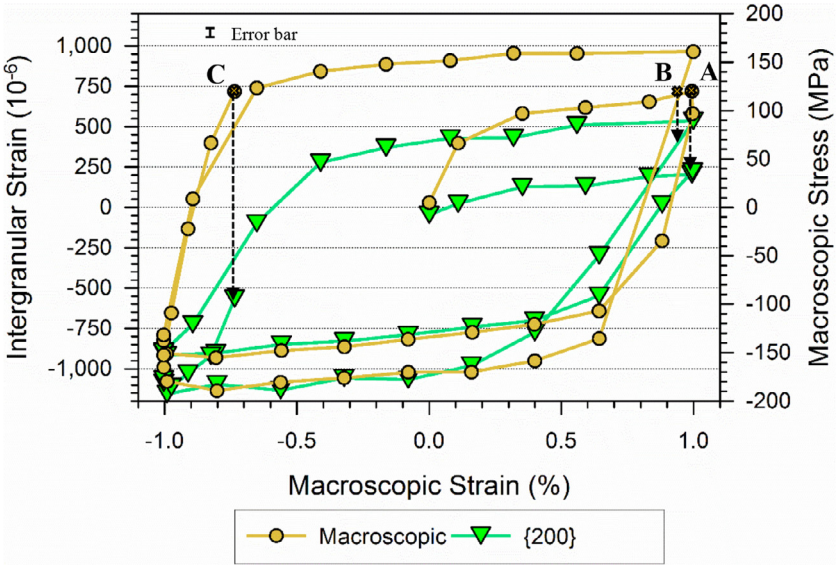

Fig. 4. Variation of axial IR strains in the {200} grain family during cyclic loading of 316H at 650 °C. Points A, B and C shows 3 positions in the cyclic loading curve where the applied stress is the same but the IR strain is different.

increased strain hardening in the material during the tension reloading in the second quarter cycle.

3.2. Effect of IR strains on the creep rate

The effect of the IR strains on the creep deformation rate is evaluated by comparing creep dwells introduced at the various points of the cyclic loading curve under the same applied macroscopic stress. The variation of IR strains is most clearly visualised in the {200} grain family as illustrated in Fig. 4. IR stresses in different grain families and different directions must satisfy equilibrium over the total volume of material. Thus it can be inferred that for an increase in tensile IR strain in one specific grain family, there must be a compensating increase in compressive IR strains in other grain families and vice versa.

The {200} IR strains for the same applied stress at points A, B and C in the cycle (as described in Fig. 1) are indicated by arrows in Fig. 4. At the peak tensile stress (120 MPa) of the first $\frac{1}{4}$-cycle (denoted point A), the {200} IR strain is 200 microstrain (in tension). At point B (120 MPa) during unloading from the peak tensile stress of the second $\frac{1}{4}$-cycle, the {200} IR strain is 400 microstrain (tension) which is higher in magnitude than for the same stress at point A. Thus the IR strains increase with repeated cycling. Lastly, at point C (120 MPa) near the end of the 2nd cycle, the {200} IR strain is 600 microstrain (compression).

Fig. 5 shows 3 creep deformation curves corresponding to an identical starting stress of 120 MPa at points A, B and C in the stress–strain loop. Each of these dwells was conducted for ~15 h, the maximum that could be accommodated within the allocated neutron beam time. As the tests were conducted at 650 °C (>0.46 T_m), a significant amount of creep strain was accumulated within this time frame. There are clear differences between levels of creep strain and also between the shapes of the creep curves; dwells at points A and C show distinct primary creep behaviour whereas the dwell at point B hardly shows any primary creep.

The creep strain rates of the dwells starting from points A and C after ~7 h of dwell are compared in Fig. 6. This is also used as the starting point for determining the minimum creep rate for the 3 dwells. The minimum creep rate of the dwell starting at point A is almost twice the rate starting at point B. Numerical values of minimum creep strain rate and IR strains for the three cases are summarised in Table 2. In order to compare the relative magnitude of IR strains at the 3 start of dwell points A, B and C, the difference between the IR strains of the most tensile and compressive grain families (difference in the IR strains of the {200} and {220} grain families in this case) has been calculated for each point.

Table 2
Creep dwell data starting from points A, B and C of Fig. 4.

Specimen and dwell start point	Start of dwell stress (MPa)	Macroscopic strain at dwell start (%)	IR strain difference between the {200} and {220} at dwell start (10^{-6})	Min. creep rate (h^{-1})
A	120	1.028	385	1.06E−04
B	120	1.022	719	4.58E−05
C	120	−0.718	535	8.90E−05

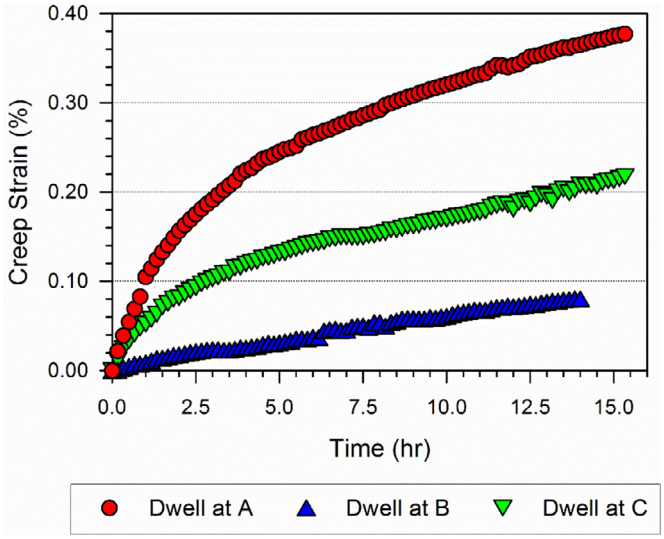

Fig. 5. Macroscopic creep dwell curves starting at 120 MPa from points A, B and C of the stress–strain loop shown in Fig. 1 and (b) differentials of the macroscopic creep strain rate with time.

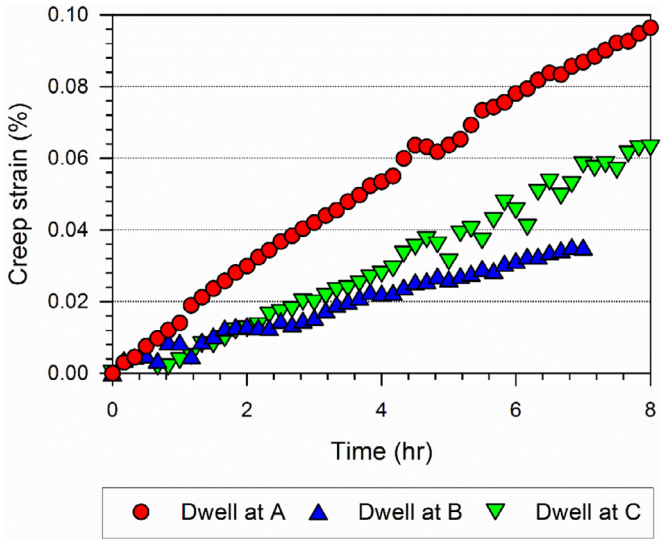

Fig. 6. Comparison of the secondary creep deformation behaviour of creep dwells started at points A, B and C of Fig. 4 (where secondary creep is taken to commence after 7 h).

Table 2 shows, the higher the range of IR strain, the slower the creep deformation rate of the dwell introduced at that point. The higher difference in the IR strain range means a greater inhomogeneity of deformation state between variously oriented grains. This reduces the effective stress dictating the creep deformation rate and therefore the creep deformation rate is reduced.

3.3. Evolution of IR strains during creep dwells

The corresponding changes in axial IR strains in the {200}, {220} and {311} grain families during the creep dwells started at points A, B and C are plotted in Figs. 7, 8 and 9, respectively. For the dwells starting at points A and B, there is little variation in IR strains throughout the creep dwells, apart from a slight increase in the {200} grain family in the first few hours for dwell A. But the magnitude of {200} grain family IR strains for dwell B is almost twice that observed for dwell A.

The axial IR strains during dwell C show an interesting variation as presented in Fig. 9. During primary creep deformation, the IR strains increase and decrease rapidly in the {200} and the {220} grain families respectively. The specimen was compressively strained at the beginning of the dwell at this point, so unlike the other two dwells, the IR strains in the {200} grain family were compressive and those in the {220} grain family were tensile. The changes of IR strains in the {200} and {220} grain family appear to approach a saturation level with time. The IR strains in the {311} grain family were compressive and remain nearly unchanged throughout the dwell.

The variations in IR strains observed during the dwell from point C are large compared with the other two dwells. This is because, from a macroscopic viewpoint, the material was close to the maximum stress in the elastic regime, when the creep dwell started. The response of the IR strains in the 3 grain families during creep deformation is observed to be similar to the response of plastic deformation, that is, an increase in tensile and compressive IR strains respectively for the {200} and the {220} grain families and negligible change for the {311} grain family. The increase in tensile IR strains in the {200} grain family during creep deformation suggests that those grains are slowest to deform compared with other grain families. This implies that during dislocation based creep deformation of type 316H austenitic steel, the set of grains which are plastically weaker and stronger are the same set of grains which are creep weaker and stronger respectively.

4. Discussion

The experimental results in this paper provide an insight into the effect of microscopic IR strains, generated from grain-scale deformation inhomogeneities, on the macroscopic creep deformation of type 316H stainless steel. They further show that, in dislocation creep regime, the set of plastic weaker grains is the same set of grains which is ‘creep weaker’ in this material. The experimental findings are discussed below with reference to the recently published multi-scale self-consistent modelling work of Petkov et al. [24].

A multi-scale self-consistent model (MSCM) has been developed by Hu and Cocks [26] describing lattice-scale deformation in austenitic type 316H stainless steel. The model has been further enhanced by Petkov et al. [24] with the incorporation of the effect of dynamic recovery allowing it to be used to predict creep deformation in austenitic stainless steels. Application of the model to predict the creep deformation behaviour of dwells A, B and C are reported in [24]. The model was first calibrated using the macroscopic monotonic elastic-plastic and cyclic stress–strain experimental data presented in Fig. 3 by adjusting the parameters controlling the initial obstacle density, self/latent hardening and dynamic recovery [24]. The 3 creep dwells, each with a duration of 15 h, were then introduced after modelling the appropriate cyclic loading history prior to reaching points A, B and C of Fig. 1. The

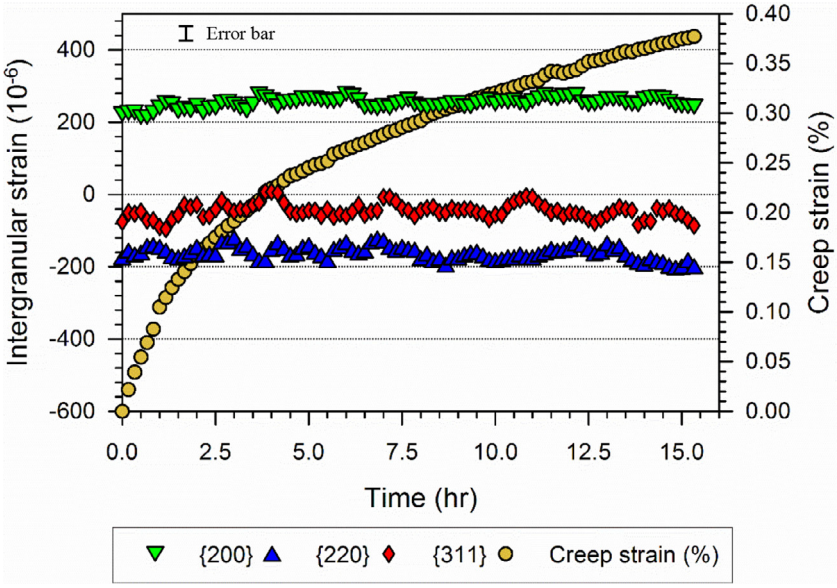

Fig. 7. Evolution of axial IR strains during creep dwells of 316H stainless steel at 120 MPa and 650 °C started at point A.

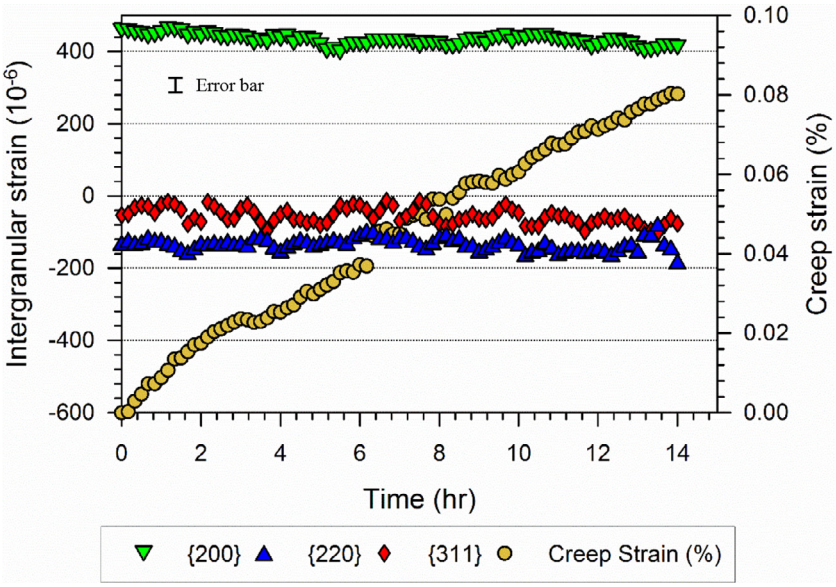

Fig. 8. Evolution of axial IR strains during creep dwells of 316H stainless steel at 120 MPa and 650 °C started at point B.

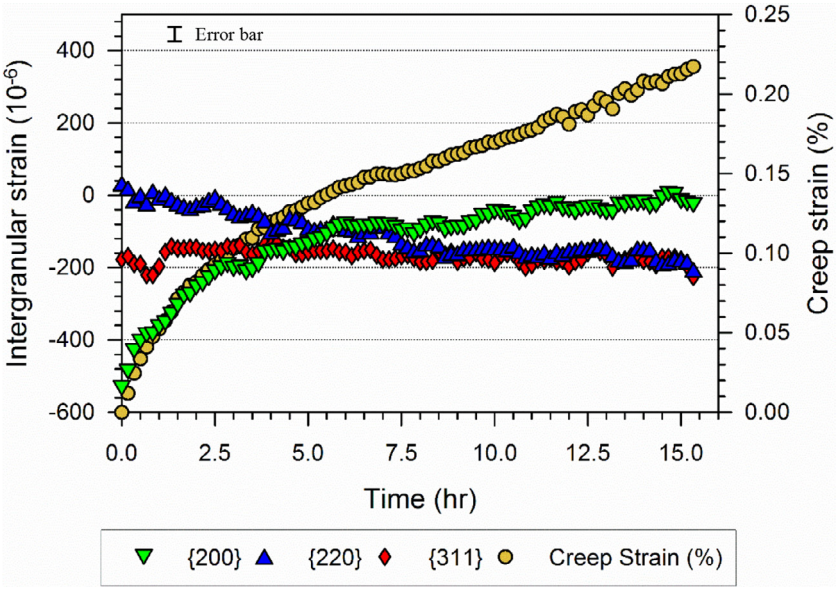

Fig. 9. Evolution of axial IR strains during creep dwells of 316H stainless steel at 120 MPa and 650 °C started at point C.

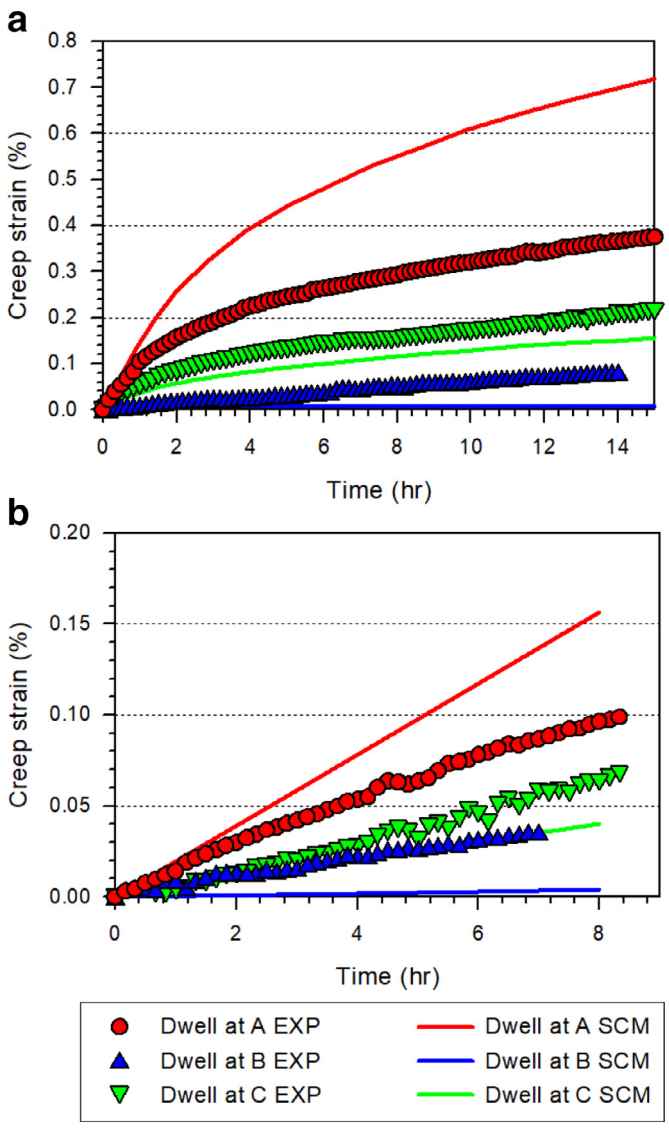

Fig. 10. Comparison of the macroscopic creep prediction curves with the MSCM prediction from [24]. (a) shows the comparison of the complete creep curves and (b) shows the comparison of the secondary portion of the creep curves.

static recovery controlling parameter of the model was calibrated using the creep response at the desired temperature upon monotonic load-up in tension (Type A history, Fig. 1).

Fig. 10 compares the macroscopic experimental data with the model prediction for creep dwells at points A, B and C. It can be observed that the model ranks the experimental trend of the 3 creep dwells, with dwell A accumulating most creep strain and dwell B the least. The model also captures the much high primary creep strain accumulation measured during dwell A, almost negligible primary creep strain accumulation during dwell B and small primary creep strain accumulation during dwell C. The magnitude of total creep strain accumulation (Fig. 10a) and minimum creep rates (Fig. 10b) predicted by the model does not match well with the experimental data.

The MSCM's prediction correlates with the experimental observation showing a reduction of minimum creep deformation rate due to prior cyclic loading (compare dwells B and C with dwell A after monotonic loading). Similar experimental observations are reported for type 316H stainless steel elsewhere, such as in [28,27]. The dislocation density at the start of dwells B and C is much higher than prior to dwell A; further movement of dislocations during dwells B and C meets stronger resistance compared to dwell A and therefore the creep rate is lower. However, the difference in the hardened state (in terms of dislocation density) of the material at the start of dwell cannot fully explain the observed differences in creep rate between the dwells. For example, although material prior to dwell C had experienced a $\frac{3}{4}$ load cycle additional to dwell B, the minimum creep rate of dwell C was found to be almost twice that of dwell B. A similar qualitative creep rate trend for these dwells is also predicted by the MSCM model as presented in Fig. 10(b); although the creep rate predicted for dwell B is much lower than the experimental data. The differences in the creep rates for these 3 dwells can be partly attributed to the difference in the IR strain state observed at the start of the dwell.

The IR strain range (calculated from the difference of IR strains in the {200} and {220} grain family) at the beginning of dwell B was greater than for dwell C followed by dwell A. Thus the minimum creep rate has an inverse relationship with IR strain range. A higher IR strain range means there is a greater magnitude of deformation inhomogeneities between variously oriented grains. In other words, at the start of dwell B, grains with one orientation are under higher tensile residual stress while grains at other orientations are under higher compressive residual stress, compared with the other 2 dwells. When a forward creep load is applied, these residual stresses act as back stress and therefore the effective stress dictating the creep deformation rate is reduced. This explanation of IR stresses acting as back stress is supported by the anelastic creep observations of Rao et al. [22] for type 316H stainless steel at 650 °C. In this case, a 24-h creep dwell at a stress of 180 MPa was followed by unloading (for 6 h) during which time negative macroscopic creep (anelastic recovery of creep strain) was observed alongside time-dependent changes in IR strains. Based on these observations, Rao et al. postulated that the IR strains and associated IR stresses were partly responsible for the observed negative creep, that is they acted as back stress in the material. Negative creep deformation and corresponding changes in IR strains were also observed in our test (the unloading part is not been presented here for brevity) which confirms the important contribution of IR strain in dictating the creep deformation rates in type 316H stainless steel. In summary, the differences in the creep deformation rate observed for dwells A, B and C arise from the combined effect of changed material hardening and the IR stress state at the beginning of the dwell. However, from the presented experimental data, it is difficult to quantitatively separate the relative contributions of the IR strains and the hardening to the observed differences in the creep rates.

Another significant observation regarding the macroscopic creep deformation behaviour was reduced primary creep for dwells preceded by cyclic loading (dwell B shows hardly any primary creep). This effect has been reported by Joseph et al. [28] for type 316H stainless steel at 550 °C. Cyclic loading is believed to reduce the spacing between dislocations and obstacles which makes static recovery by dislocation climb processes faster [29]. This accelerates the balance between hardening and recovery [30] and thereby promotes early secondary creep behaviour. Although this explains lower primary creep strain accumulation during dwells B and C compared to dwell A, it does not explain the complete lack of primary creep in dwell B. MSCM modelling results of Petkov et al. [24] show only a minor difference in the resultant dislocation – obstacle spacing between the start of dwell B and dwell C. Petkov et al. suggest that the lack of primary creep in dwell B is due to a type II residual stress field generated at the peak tensile strain position of the 2nd cycle, which allows for compatible plastic deformation during the subsequent tensile creep dwell. But this explanation is inadequate since a very similar residual stress field (only different in terms of magnitude) was observed at peak tensile strain in the 1st and 2nd cycle and a significant primary creep was observed in dwell A introduced at the peak tensile strain in the 1st cycle.

We believe that the lack of primary creep during dwell B is because of a high-level of dislocation tangling at the beginning of this creep dwell. The occurrence of primary creep not only depends on the dislocation density but also on the arrangement of dislocations and

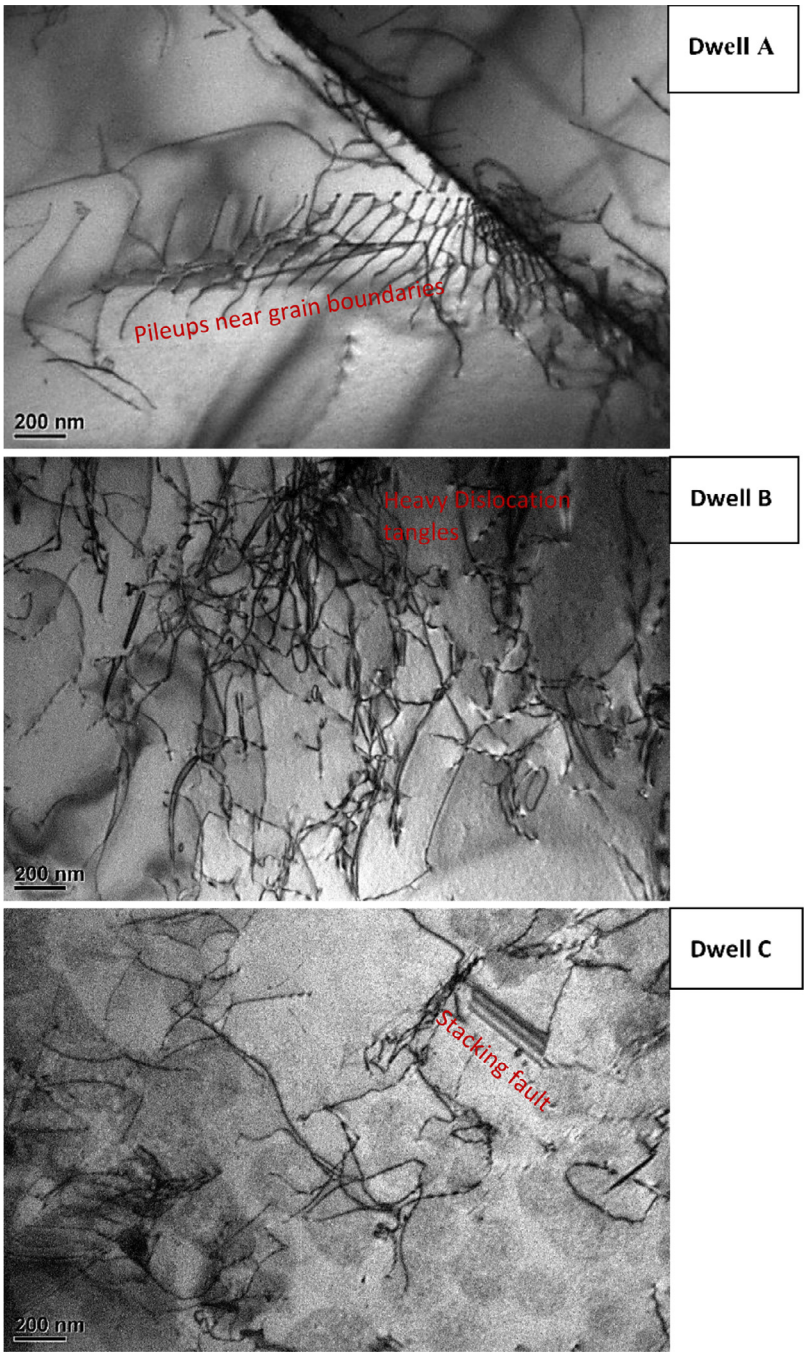

Fig. 11. Representative examples of observed dislocation structures in material samples prior to the start of creep dwells A, B and C obtained using the bright field transmission electron microscopy technique.

interactions with mobile dislocations and other obstacles, such as the solute elements and second-phase precipitates. A qualitative dislocation analysis was conducted using interrupted samples at the start of the 3 dwells; a representative image of this analysis for each of the dwell types is presented in Fig. 11. The observed dislocation structures at the beginning of the 3 dwells are distinct from each other. Type 316H stainless steel has low stacking fault energy, therefore the observed features of planar slip such as dislocation pile-ups near the grain boundary and the stacking faults are expected after monotonic and cyclic plastic loading. Unlike the other two dwells, a heavy dislocation tangling and a lack of stacking faults can be observed in sample material prior to dwell B. A similar observation regarding the formation of dislocation tangling due to cyclic loading in type 316L stainless steel [31] has been reported. The dislocation tangling limits the number of mobile dislocations required for primary creep and therefore, no primary creep is observed for the dwell. Some of the dislocations untangled during the reverse plastic loading in compression in the 3rd cycle and therefore, less severe tangling can be observed prior to dwell C resulting in the observed return of primary creep stage during this dwell.

The axial IR strains during load-controlled creep dwells were observed to remain nearly unchanged for dwells A and B but significantly evolved during the dwell C. This is because at the start of dwell C, although the material was cyclically hardened it was deforming elastically and therefore, the elastic lattice strains in different grain families evolved during creep. During this load-controlled dwell, increasing tensile and compressive IR strains in the {200} and the {220} grain families respectively (Fig. 9) imply that the elastic lattice strains in the {200} grain families were increasing while those in the {220} grain families were decreasing. This redistribution of strains between grains is postulated to be partly controlling the accumulation of inelastic strain during

the primary creep stage [24]. Further modelling work is required to quantify the effect of the redistribution of lattice strains between grain families on the macroscopic creep strain accumulation; this will be part of a future publication.

A number of other important insights arise from the observed evolution of IR strains during the creep dwells. Recent studies on creep deformation of type 316H stainless steel at 550 °C have concluded that the lattice strains during load-controlled creep dwell remain constant [32], however, our results clearly show that this is not the case. The lattice strains in different grain families evolve significantly during load-controlled creep dwell if the dwell is introduced before reaching the cyclic yield stress of the material. In another recent creep study on type 316H stainless steel at 550 °C, Chen et al. [21] concluded that the magnitude of IR strains between different grain families is a function of the total inelastic strain accumulated in the material. This conclusion is not supported by the results presented here where the magnitude of IR strains only evolves during dwell C. Our experiment shows that whereas for plastic deformation the magnitude of IR stains is a function of the accumulated strain, for creep deformation it is much more complex. This is because, during plastic deformation, the IR strains are accumulated depending on the material's inherent elastic and plastic anisotropy, whereas during creep deformation we postulate that there is no inherent 'creep anisotropy'. It appears that the accumulation/relaxation of IR strains during creep is heavily dictated by the magnitude and nature of prior plasticity generated IR strains and elastoplastic deformation state of the material at which the creep dwell is introduced. From the evolution of the IR strains in different grain families during creep dwell C, a comparison of the IR strain evolution during creep and plasticity can be drawn. In dwell C, with increasing creep strain, the {200} grain families accumulate tensile IR strain, the {220} grain families accumulate compressive IR strain and the {311} grain families accumulate negligible IR strain. Interestingly, similar behaviour in these 3 grain families would be expected if a tensile 'plastic' deformation was applied instead of 'creep' deformation at this point of loading. This suggests that IR strain evolution during dwell C is more of a plasticity driven phenomenon rather than creep driven.

It is important to mention that the experimental results in this study are limited by the overly short duration of creep dwells examined which were constrained by limited access to neutron beam time for in-situ testing. Further tests with longer duration creep dwells are required to confirm the findings regarding the evolution of IR strains during primary and secondary creep deformation stages. Furthermore, these results only represent the earlier stages of creep deformation in type 316H, prior to the formation of significant precipitates and dislocation cell structures.

5. Conclusions

Novel experimental work has been presented investigating the effect of cyclic plasticity on the subsequent creep deformation of type 316H stainless steel and its interpretation based upon recently developed multi-scale self-consistent model predictions. The test results show that creep deformation behaviour during interrupted creep dwells is not only dependent on the applied stress but also on the materials hardened and underlying micro-scale plastic strain state. This is important because low cycle creep-fatigue loading with intermediate creep dwells is commonly experienced by power generation plant during routine operations. Current creep life assessment procedures simplistically use the start of dwell stresses to calculate creep dwell deformation which can lead to overly conservative estimates. The present work shows that IR strains, which contribute to accelerating/decelerating creep deformation rates, need to be accounted for, potentially using micro-mechanical deformation models. The experimentally measured lattice strain responses of differently oriented grain families during creep deformation, after various plastic deformation cycles, can be used to validate any crystal plasticity based or self-consistent based micro-mechanical model.

The following insights have been obtained from the work:

1. The creep deformation rates of load-controlled creep dwells introduced at various common stress level positions during tension-compression cyclic loading of type 316H stainless steel were found to differ owing to the intergranular strain state at the start of dwell.
2. Prior cyclic plastic loading was found to reduce the minimum creep deformation rate as well as the magnitude of primary creep strain. The extent of the effect depends on the position in the cycle at which the creep dwell is introduced.
3. The evolution of intergranular strains during creep deformation depends on the elastic-plastic deformation state at the position where creep dwell is introduced, and not the total inelastic strain accumulation in the material (reported by others).
4. During load-controlled tensile creep dwells, intergranular strains were found to remain nearly unchanged during dwells introduced after cyclic yielding in the tensile direction but to evolve significantly during an intermediate creep dwell starting before cyclic yield.
5. Comparing the evolution of intergranular strains in various grain families during plastic and creep deformation, it was found that the grain families which deformed relatively more or less during plastic deformation behaved similarly during creep deformation.

Acknowledgements

We would like to acknowledge the funding for this research work from EDF Energy Nuclear Generation Ltd, UK. Abdullah Al Mamun is grateful to Open University for accommodating his Ph.D. studentship. We would also like to thank the STFC, ISIS facility for the award of the neutron beam time (experiment no. 1410292) and funding for conducting the experiment.

Declaration of interest

The authors declare no conflict of interest.

References

[1] R5, Assessment Procedure for the High Temperature Response of Structures Issue 3, Revision 002, EDF Energy, Gloucester, UK, 2014.
[2] ASME-BPVC-SEC 3 NH-2013 - Section 3 - Rules for Construction of Nuclear Power Plant Components - Division 1 - Subsection NH - Class 1 Components in Elevated Temperature Service, ASME New York USA, 2013.
[3] S. Holdsworth, Creep-fatigue failure diagnosis, Materials 8 (2015) 7757–7769.
[4] M.W. Spindler, Effects of dwell location on the creep-fatigue endurance of cast type 304L, Mater. High Temp. 25 (2008) 187–196.
[5] B. Chen, P.E.J. Flewitt, A.C.F. Cocks, D.J. Smith, A review of the changes to internal state related to high temperature creep of polycrystalline metals and alloys, Int. Mater. Rev. 60 (2015) 1–29.
[6] D.F. Li, N.P. O'Dowd, C.M. Davies, K.M. Nikbin, A review of the effect of prior inelastic deformation on high temperature mechanical response of engineering alloys, Int. J. Press. Vessel. Pip. 87 (2010) 531–542.
[7] B.F. Dyson, Microstructure based creep constitutive model for precipitation strengthened alloys: theory and application, Mater. Sci. Technol. 25 (2009) 213–220.
[8] F.P.E. Dunne, A.M. Othman, F.R. Hall, D.R. Hayhurst, Representation of uniaxial creep curves using continuum damage mechanics, Int. J. Mech. Sci. 32 (1990) 945–957.
[9] A.F. Bower, E. Wininger, A two-dimensional finite element method for simulating the constitutive response and microstructure of polycrystals during high temperature plastic deformation, J. Mech. Phys. Solids 52 (2004) 1289–1317.
[10] T.O. Erinosho, K.A. Venkata, M. Mostafavi, D.M. Knowles, C.E. Truman, Influence of prior cyclic plasticity on creep deformation using crystal plasticity modelling, Int. J. Solids Struct. 139-140 (2018) 129–137.
[11] H. Altenbach, K. Naumenko, Modelling of Creep For Structural Analysis, V.I. Babitsky, J. Wittenburg (Eds.), Springer, 2007.
[12] H. Ishikawa, K. Sasaki, Unified approach to constitutive modelin -plasticity and creep, Advances in Engineering Plasticity and its Applications, 1996 Hiroshima, Japan.
[13] F. Dobes, The back stresses in creep of a Fe–30Al–4Cr intermetallic alloy with addition of Zr, Scr. Mater. 59 (2008) 59–62.
[14] H. Takagi, M. Dao, M. Fujiwara, M. Otsuka, Experimental and computational creep characterization of Al–Mg solid-solution alloy through instrumented indentation, Philos. Mag. 83 (2003) 3959–3976.
[15] A.A. Mamun, R.J. Moat, J. Kelleher, P.J. Bouchard, Origin of the Bauschinger effect in a polycrystalline material, Mater. Sci. Eng.: A 707 (2017) 576–584.
[16] W.D. Nix, J.C. Gibeling, K.P. Fuchs, The Role of Long -range internal Back Stresses in Creep of Metals, ASTM Special Technical Publication, 1982, pp. 301–321.

[17] B. Chen, J.N. Hu, Y.Q. Wang, S. Kabra, A.C.F. Cocks, D.J. Smith, P.E.J. Flewitt, Internal strains between grains during creep deformation of an austenitic stainless steel, J. Mater. Sci. 50 (2015) 5809–5816.
[18] A.A. Mamun, R.J. Moat, P.J. Bouchard, Origin and effect of back stress on cyclic creep deformation of 316H stainless steel, in: Proceedings of ASME 2015 Pressure Vessels and Piping Conference, Boston, USA, 2015.
[19] D.-F. Li, C.M. Davies, S.-Y. Zhang, C. Dickinson, N.P. O'Dowd, The effect of prior deformation on subsequent microplasticity and damage evolution in an austenitic stainless steel at elevated temperature, Acta Mater. 61 (2013) 3575–3584.
[20] M.R. Daymond, P.J. Bouchard, Elastoplastic deformation of 316 stainless steel under tensile loading at elevated temperatures, Metall. Mater. Trans. A 37 (2006) 1863–1873.
[21] B. Chen, J.N. Hu, P.E.J. Flewitt, D.J. Smith, A.C.F. Cocks, S.Y. Zhang, Quantifying internal stress and internal resistance associated with thermal ageing and creep in a polycrystalline material, Acta Mater. 67 (2014) 207–219.
[22] A. Rao, P.J. Bouchard, S.M. Northover, M.E. Fitzpatrick, Anelasticity in austenitic stainless steel, Acta Mater. 60 (2012) 6851–6861.
[23] Y.Q. Wang, S. Hossain, S. Kabra, S.Y. Zhang, D.J. Smith, C.E. Truman, Effect of boundary conditions on the evolution of lattice strains in a polycrystalline austenitic stainless steel, J. Mater. Sci. 52 (2017) 7929–7936.
[24] M.P. Petkov, J. Hu, A.C.F. Cocks, Self-consistent modelling of cyclic loading and relaxation in austenitic 316H stainless steel, Philos. Mag. 99 (2019) 1–46.
[25] J.R. Santisteban, M.R. Daymond, J.A. James, L. Edwards, ENGIN-X: a third-generation neutron strain scanner, J. Appl. Crystallogr. 39 (2006) 812–825.
[26] J. Hu, A.C.F. Cocks, A multi-scale self-consistent model describing the lattice deformation in austenitic stainless steels, Int. J. Solids Struct. 78-79 (2016) 21–37.
[27] B. Wilshire, M. Willis, Mechanisms of strain accumulation and damage development during creep of prestrained 316 stainless steels, Metall. Mater. Trans. A 35A (2004) 563–571.
[28] T.D. Joseph, D. Mclennon, M.W. Spindler, C.E. Truman, D.J. Smith, The effect of prior cyclic loading variables on the creep behaviour of ex-service type 316H stainless steel, Mater. High Temp. 30 (2013) 156–160.
[29] D.G. Morris, D.R. Harries, Recovery of a creep-deformed type 316 stainless steel, J. Mater. Sci. 14 (1979) 2625–2636.
[30] O. Ajaja, A.J. Ardell, The Effect of Prior Cold Work on the Creep Characteristics of AISI Type 304 Stainless Steel, Ecole Nationale Superieure de la Metallurgie et de l'Industrie des Mines Laboratoire de Physique du Solide, France, 1976.
[31] M.S. Pham, C. Solenthaler, K.G.F. Janssens, S.R. Holdsworth, Dislocation structure evolution and its effects on cyclic deformation response of AISI 316L stainless steel, Mater. Sci. Eng.: A 528 (2011) 3261–3269.
[32] Y.Q. Wang, M.W. Spindler, C.E. Truman, D.J. Smith, Critical analysis of the prediction of stress relaxation from forward creep of type 316H austenitic stainless steel, Mater. Des. 95 (2016) 656–668.